The Astrophysical Journal Supplement Series, 186:85–93, 2010 January doi:10.1088/0067-0049/186/1/85

RADIATIVE L-SHELL TRANSITIONS IN Fe XIX AND Fe XX IONS

S. Kotochigova[1], M. Linnik[1], K. P. Kirby[2], and N. S. Brickhouse[3]
[1] Department of Physics, Temple University, Philadelphia, PA 19122, USA
[2] Institute for Theoretical Atomic Molecular and Optical Physics, Harvard-Smithsonian Center for Astrophysics, 60 Garden Street, Cambridge, MA 02138, USA
[3] Harvard-Smithsonian Center for Astrophysics, 60 Garden Street, Cambridge, MA 02138, USA
Received 2009 September 21; accepted 2009 November 10; published 2009 December 22

ABSTRACT

We compute the wavelengths and oscillator strengths for the $3s$, $3d \rightarrow 2p$, and $3p \rightarrow 2s$ emission lines in Fe XIX and Fe XX ions by using a configuration interaction Dirac–Fock and Dirac–Fock–Sturm method combined with second-order Brillouin–Wigner perturbation theory. We provide a complete list of computed wavelengths and oscillator strengths in both the velocity and length gauge for these transitions, many of which have never previously been reported. A comparison of our data with laboratory measurements and other theoretical predictions allows us to estimate an uncertainty of ∼2 mÅ in the wavelengths and an uncertainty of 2%–3% in the oscillator strengths. We expect that our calculations will provide a means of identifying emission lines from astrophysical sources and improve the ability to detect blending in X-ray grating spectra from *Chandra* and *XMM-Newton*. As an example, we present a simulated emission spectrum of Capella and find improved agreement between the observations and our calculations, compared with previous data sets.

Key words: atomic data – atomic processes – line: identification – X-rays: general

Online-only material: color figures

1. INTRODUCTION

In response to significant advances in the quality of astrophysical X-ray observations, a number of high-accuracy theoretical calculations of the atomic structure (and spectroscopy) of highly stripped ions have been initiated over the last few years (e.g., Gu 2005; Kotochigova et al. 2007; Chen 2008).

In addition to H- and He-like K-shell lines of cosmically abundant elements from carbon to iron, Fe L-shell lines between 10 and 18 Å are often observed at high spectral resolution in the X-ray grating spectra from *Chandra* and *XMM-Newton*. Fe L-shell lines are observed from a diversity of sources, including stellar coronae, hot star winds, elliptical galaxies, and cataclysmic variables in emission, and active galactic nuclei (AGNs) and X-ray binaries in absorption. These lines provide important diagnostics for the temperature, density, charge state, and elemental abundance of the gas.

In this study, we focus on numerical calculations of wavelengths and oscillator strengths for the iron ions Fe XIX and Fe XX. Accurate calculations of wavelengths are motivated by benchmark studies of astrophysical plasmas, in particular using the in-flight grating calibration spectra of the stellar coronal binary Capella (Canizares et al. 2000; Brinkman et al. 2001). The summed spectra of the accumulated *Chandra* High Energy Transmission Grating (HETG) observations of Capella are particularly useful for testing spectral models for lines produced near 6 MK (where the emission measure distribution peaks), since they provide high signal-to-noise ratios at the highest resolving power currently available (∼0.014 Å instrumental FWHM with the High Energy Grating). Comparisons between the Capella data and spectral models produced by the APEC v1.3 code (Smith et al. 2001) show generally good agreement for the strongest lines, but a number of issues have arisen. For example, Figure 1 shows a comparison between the observed Capella spectrum between 13.4 and 13.8 Å and three models using different wavelengths for the Fe XIX lines. This spectral region is of great interest because it contains the He-like diagnostic lines of Ne IX, along with a number of Fe XIX lines. In the upper panel of Figure 1, iron wavelengths calculated by D. Liedahl (1997, private communication) appear offset from the observations and do not reproduce all of the structure. The middle panel shows a comparison with the standard APEC model, which replaces the HULLAC wavelengths with the experimental wavelengths reported by Brown et al. (2002), where available. This model reduces the offset for the shorter wavelengths, but the wavelengths still do not match at the longer wavelengths (Ness et al. 2003). Finally, the lower panel shows good agreement throughout the region, as well as a clear one-to-one correspondence between observed and model features. Given such good agreement, one can be confident that the Ne IX diagnostic lines are not strongly affected by blending with Fe XIX.

Iron lines from other regions of the spectrum are reported in Desai et al. (2005). They find discrepancies between APEC and the Capella observations at longer wavelengths, and suggest that some of the experimental lines may have been misidentified. Misidentification of experimental lines is not unexpected, given heavy blending and the inaccuracy of the theoretical models available at the time of the experiments. We expect that the calculations presented in this paper will greatly improve the assessment of blending for diagnostic lines of interest and the utility of the iron lines themselves.

Accurate wavelengths are needed for identification and deblending of emission lines not only in collisionally ionized plasmas such as the corona of Capella, but also for understanding emission and absorption lines produced in photoionized plasmas. Accurate oscillator strengths are important especially for photoionized plasmas, where radiative processes dominate. In the AGN NGC 3783 numerous absorption lines of Fe XIX and Fe XX are identified (Krongold et al. 2003), while identification of lines from these ions is less secure in the galactic black hole Cygnus X-1 (Miller et al. 2005). Even in collisionally ionized plasmas where the line emission processes are dominated by collisional excitation, radiative transition rates can be important for calculating the emission produced by the decay of metastable

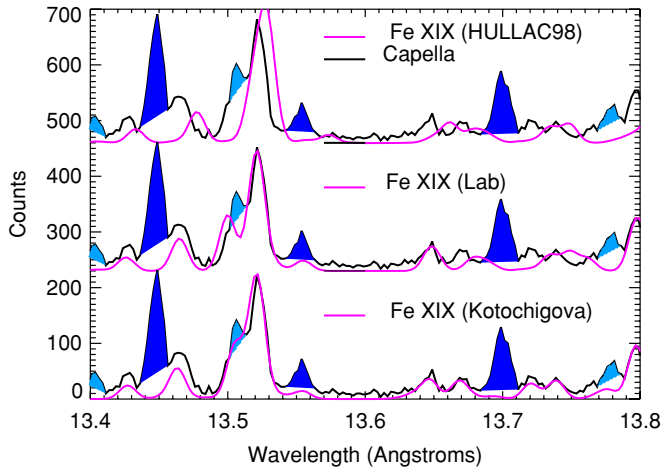

Figure 1. *Chandra* spectrum of Capella (black line) in the spectral region between 13.4 and 13.8 Å (Desai et al. 2005) shown in comparison with three spectral models. The three models for Fe XIX (in magenta) use data from the APEC code v1.3 (Smith et al. 2001) with only the wavelengths changed. Ne IX (dark blue) and other Fe L-shell (light blue) lines in the region are shaded for the observed spectrum. Upper panel: model using the Fe XIX wavelengths from HULLAC (D. Liedahl 1997, private communication). Middle panel: Fe XIX wavelengths include the experimentally measured values reported in Brown et al. (2002). Lower panel: Fe XIX wavelengths are from this work and Kotochigova et al. (2007) using the MDFS method. Adapted from Brickhouse (2007).

(A color version of this figure is available in the online journal.)

states. Accurate atomic data are also critical for determining the velocity structure in the presence of complex line blending (Pollock et al. 2005).

We use a relativistic atomic structure software suite of codes described in an earlier study of Kotochigova et al. (2007) to perform numerical calculations of wavelengths and oscillator strengths of the X-ray transitions involving the $2s$, $2p$, $3s$, $3p$, and $3d$ levels of Fe XIX and Fe XX. Primary attention is given to accurate and complete atomic data for the L-shell transitions. We compare our results to experimental atomic data obtained by Brown et al. (2002) and Shirai et al. (2000) as well as to other theoretical studies reported by Brown et al. (2002) and Gu (2005).

2. DESCRIPTION OF CALCULATIONS

We present calculations of the $2p^{q-1}3s, 3d \rightarrow 2p^q$, and $2s2p^q3p \rightarrow 2s^22p^q$ transitions in Fe XIX and Fe XX with $q = 4$ and 3, respectively. Our initial studies of the $2p^33s, 3d \rightarrow 2p^4$ transitions in Fe XIX were presented in a previous paper (Kotochigova et al. 2007). Here, we further analyze these transitions and expand our calculations to other transitions in Fe XIX and Fe XX. For these calculations, we use the ab initio configuration interaction (CI) Dirac–Fock–Sturm (MDFS) method combined with second-order Brillouin–Wigner perturbation theory (BWPT; Lennard-Jones 1930; Brillouin 1932; Wigner 1935; Hubac & Wilson 2000) with a full implementation of relativistic, correlation, and quantum electrodynamic effects. For each electronic state, spatially localized single-electron orbitals are optimized using the Dirac–Fock method. These orbitals are then used in the construction of configuration state functions (CSFs) as linear combinations of Slater determinants. Orbital functions of the occupied $1s, 2s, 2p, 3s, 3p$, and $3d$ subshells are obtained from the Dirac–Fock calculations, whereas the unoccupied $4s, 4p, 4d, 4f, 5s, 5p, 5d, 5f, 6s, 6p, \ldots$ up to $8d$ orbitals are obtained by solving the Dirac–Fock–Sturm equations. CSFs for the calculation of the initial and final state have been separately optimized. Consequently, the CSFs used to calculate the transition properties are nonorthogonal. This complicates the evaluation of the oscillator strength but in the end leads to more accurate data. The non-orthogonal four-component Dirac–Fock

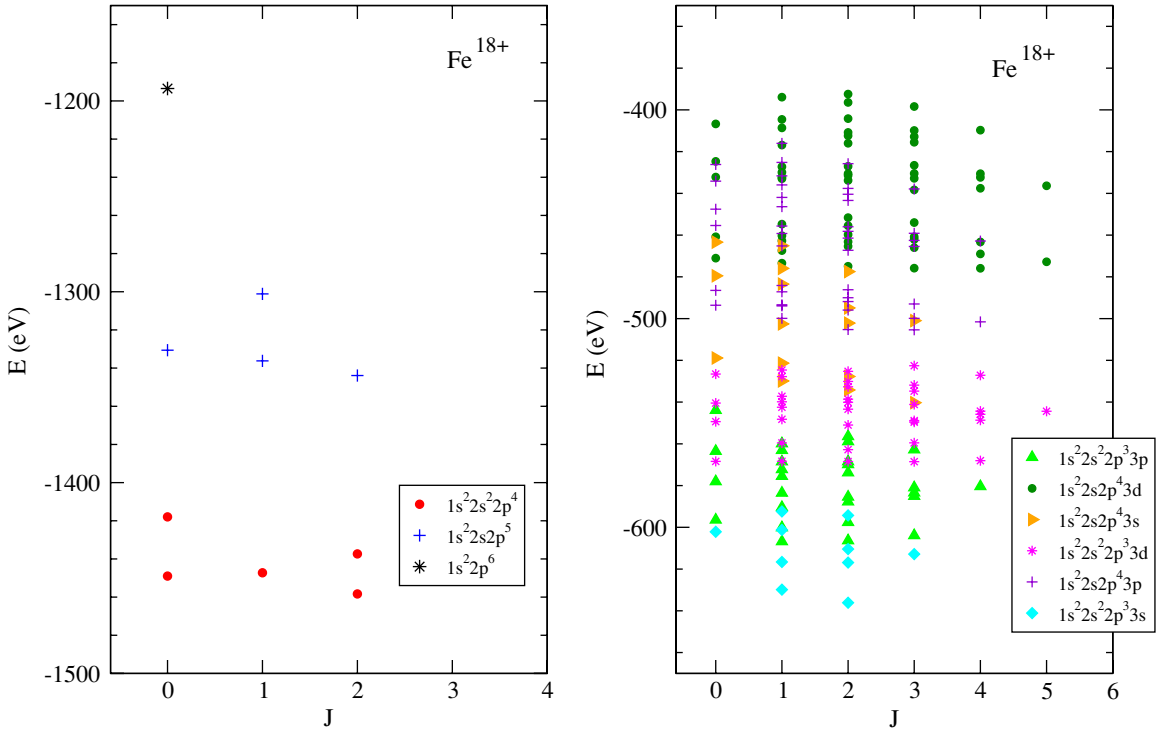

Figure 2. Binding energies for Fe^{18+} levels with respect to its ionization limit, corresponding to the Fe^{19+} ion at a total energy $E_{tot} = -27{,}163.938$ eV plus a free electron at rest. Ground and low-lying states are shown in the left panel and higher-lying states in the right panel.

(A color version of this figure is available in the online journal.)

Table 1
X-ray Wavelengths and Oscillator Strengths of Fe XIX

J	J'	λ (Å)	$f_{\rm velocity}$	$f_{\rm length}$	J	J'	λ (Å)	$f_{\rm velocity}$	$f_{\rm length}$
$1s^2\,2s^1\,2p^4\,3p \rightarrow 1s^2\,2s^2\,2p^4$									
1	2	12.0058	0.00009	0.00009	1	1	12.6116	0.00358	0.00358
2	2	12.0702	0.00027	0.00029	1	0	12.6256	0.00480	0.00480
1	2	12.0930	0.00091	0.00091	1	1	12.6481	0.00058	0.00058
1	0	12.1155	0.00105	0.00105	1	0	12.6685	0.02591	0.02589
1	1	12.1362	0.00118	0.00118	1	0	12.7107	0.00267	0.00265
1	2	12.1664	0.00138	0.00138	1	1	12.7334	0.00387	0.00387
2	1	12.2015	0.03253	0.03376	1	0	12.7346	0.00018	0.00018
1	0	12.2043	0.01491	0.01489	1	2	12.7395	0.02366	0.02359
3	2	12.2151	0.05603	0.05808	1	2	12.7767	0.01464	0.01460
2	2	12.2193	0.00284	0.00298	1	0	12.8007	0.14013	0.13948
1	1	12.2253	0.00158	0.00158	1	2	12.8159	0.00000	0.00000
1	2	12.2274	0.00407	0.00406	2	2	12.8385	0.00213	0.00214
0	1	12.2282	0.00292	0.00299	1	2	12.8447	0.00001	0.00001
2	2	12.2517	0.01882	0.01935	2	2	12.8514	0.00114	0.00119
1	2	12.2546	0.00673	0.00672	1	0	12.8571	0.02269	0.02261
2	2	12.2742	0.00713	0.00747	1	2	12.8638	0.04173	0.04160
1	0	12.2790	0.00997	0.00998	2	2	12.8847	0.09978	0.10130
1	2	12.2884	0.00029	0.00029	3	2	12.8909	0.06447	0.06585
1	1	12.3003	0.01797	0.01792	1	2	12.9285	0.02539	0.02530
2	2	12.3216	0.00026	0.00022	2	2	12.9308	0.01314	0.01335
0	1	12.3236	0.00262	0.00273	1	2	12.9361	0.03509	0.03497
1	2	12.3400	0.00197	0.00197	1	0	12.9409	0.23373	0.23267
1	0	12.3411	0.00295	0.00295	2	1	12.9582	0.15370	0.15630
1	2	12.3455	0.00005	0.00005	1	1	12.9655	0.01656	0.01651
2	1	12.3539	0.03631	0.03760	1	0	12.9703	0.02893	0.02870
1	1	12.3633	0.00060	0.00060	0	1	12.9833	0.02973	0.03001
2	1	12.3870	0.00076	0.00077	3	2	12.9838	0.10920	0.11130
1	0	12.4032	0.06421	0.06421	1	1	12.9941	0.07500	0.07460
2	1	12.4100	0.03055	0.03136	1	0	12.9989	0.00069	0.00069
1	2	12.4219	0.00075	0.00075	2	1	13.0004	0.00620	0.00629
1	1	12.4249	0.00037	0.00037	1	2	13.0176	0.00584	0.00581
2	2	12.4342	0.00009	0.00006	2	1	13.0345	0.00155	0.00163
2	2	12.4521	0.01570	0.01591	1	0	13.0374	0.00012	0.00011
1	0	12.4562	0.00441	0.00439	1	0	13.0557	0.01071	0.01066
3	2	12.4615	0.00039	0.00047	2	2	13.0568	0.00619	0.00627
1	2	12.4709	0.00525	0.00524	3	2	13.0583	0.00619	0.00625
3	2	12.4727	0.02574	0.02653	1	0	13.0634	0.00132	0.00131
2	2	12.4771	0.00387	0.00377	0	1	13.0653	0.00059	0.00059
1	1	12.4781	0.01747	0.01744	1	1	13.0798	0.00111	0.00111
0	1	12.4808	0.00630	0.00654	2	1	13.0816	0.02726	0.02772
1	2	12.4855	0.00512	0.00508	1	1	13.0875	0.00225	0.00225
2	2	12.4927	0.00726	0.00753	1	2	13.0998	0.00008	0.00008
1	0	12.4945	0.01342	0.01343	2	2	13.0937	0.00001	0.00000
3	2	12.5059	0.02272	0.02316	1	0	13.1284	0.00213	0.00210
1	2	12.5066	0.00214	0.00213	1	2	13.1299	0.00001	0.00001
2	2	12.5108	0.00884	0.00932	2	2	13.1369	0.00001	0.00001
2	2	12.5343	0.00626	0.00643	1	0	13.1465	0.00022	0.00021
3	2	12.5425	0.00162	0.00169	1	1	13.1709	0.00000	0.00000
1	2	12.5491	0.00082	0.00082	1	2	13.2174	0.00068	0.00068
2	2	12.5657	0.00275	0.00283	1	2	13.2253	0.00063	0.00063
2	1	12.5736	0.00490	0.00486	1	2	13.3105	0.00013	0.00013
0	1	12.5868	0.01895	0.01902	1	0	13.3742	0.01746	0.01743
1	0	12.5889	0.17921	0.17878	1	0	13.4061	0.00015	0.00014
1	0	12.5889	0.02518	0.02513	1	0	13.4969	0.00163	0.00163
1	2	12.5900	0.00735	0.00733	1	0	13.5051	0.00054	0.00055
2	1	12.5920	0.00135	0.00137	1	0	13.5939	0.00028	0.00028
1	2	12.6032	0.00002	0.00002					

Note. X-ray wavelengths and oscillator strengths for all transitions from fine structure levels of the excited $1s^2 2s^1 2p^4 3p$ configuration to those of the $1s^2 2s^2 p^4$ ground configuration of Fe XIX. Columns labeled J and J' describe the total electron angular momentum of the excited and ground states, respectively. The columns labeled λ, $f_{\rm velocity}$, and $f_{\rm length}$ are the transition wavelengths (in Angstrom) and oscillator strengths in the velocity and length gauge, respectively.

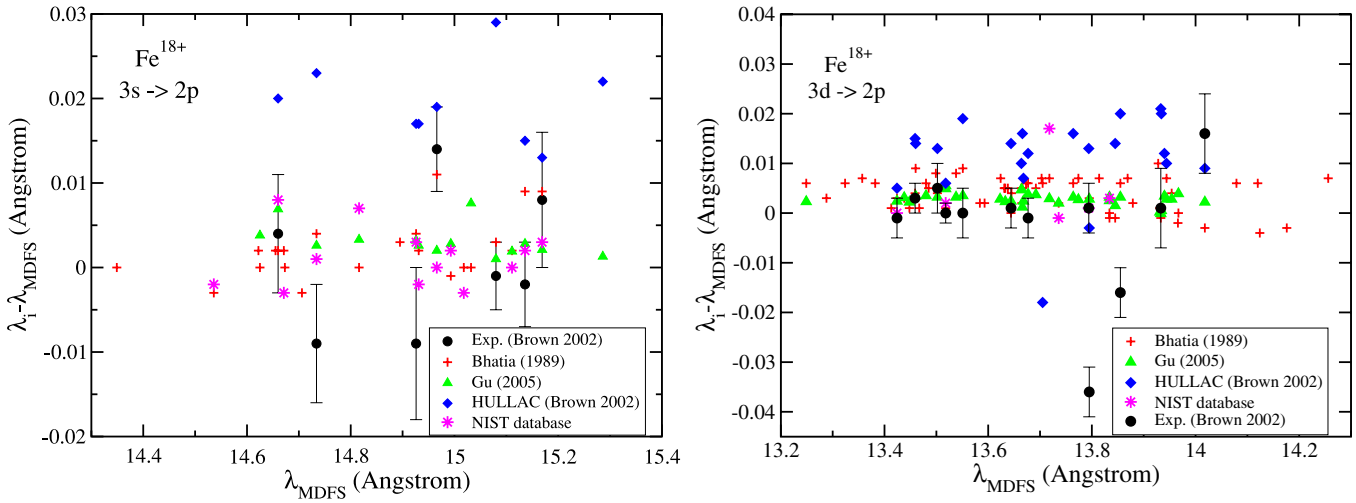

Figure 3. Differences in wavelengths of the $1s^2 2s^2 2p^2 3s \rightarrow 1s^2 2s^2 2p^3$ and $1s^2 2s^2 2p^2 3d \rightarrow 1s^2 2s^2 2p^3$ transitions in Fe^{18+} between our theoretical calculations and experimental and other theoretical results. The wavelengths of the markers labeled Exp. and HULLAC can be found in Brown et al. (2002). The markers labeled Bhatia (1989), Gu (2005), and NIST database are from Bhatia et al. (1989), Gu (2005), and Shirai et al. (2000), respectively.

(A color version of this figure is available in the online journal.)

Table 2
The Total Energies, Breit Interaction, Frequency-dependent Breit Interaction, and Quantum Electrodynamic Corrections of the Five Ground $1s^2 2s^2 2p^3$ State Levels of Fe XX

J	Total Energy	Breit	Freq. Breit	QED
1.5	−998.2559514	0.3577103	−0.0009046	0.2930876
1.5	−997.6231604	0.3597699	−0.0008297	0.2927754
2.5	−997.4522716	0.3589992	−0.0007322	0.2923720
0.5	−997.0672193	0.3574490	−0.0009232	0.2931663
1.5	−996.7801232	0.3550537	−0.0008680	0.2929264

Note. Corrections are included in the total energies. All energies are given in atomic units.

orbitals and relativistic Sturmian wave function are obtained by self-consistent field calculation for the initial and the final state of each dipole transition independently. As a result, these atomic orbitals are physically realistic leading to a compact description of an atom and to an efficient CI procedure. We determine the oscillator strength in both length and velocity gauge. In a fully converged calculation, the two results will agree indicating the overall accuracy of the wave functions. We include the effect of the finite size of the Fe nucleus, which has a nonzero effect on orbitals of s and p symmetry. The iron ions considered in this paper have open electron shells in both the initial and final states of the transitions. For quantitative agreement between experiment and theory, we perform a large-scale CI calculation. More details about the computational method can be found in Kotochigova et al. (2007).

2.1. Analysis of the Fe XIX Data

Figure 2 shows the total energy of levels in Fe XIX ion relevant for the X-ray transitions of interest in this paper. The levels are grouped and labeled by the configuration with the largest CI coefficient. The ground state configuration of Fe XIX is $1s^2 2s^2 2p^4$. For the excited states, there is one electron excited from either the $2s$ or $2p$ shell and placed in the $n = 3$ shell. The energy separation is about 900 eV. The 200 eV substructure in the two panels of Figure 2 is due to a redistribution of the electrons between the nominally degenerate $2s$ and $2p$ shells as

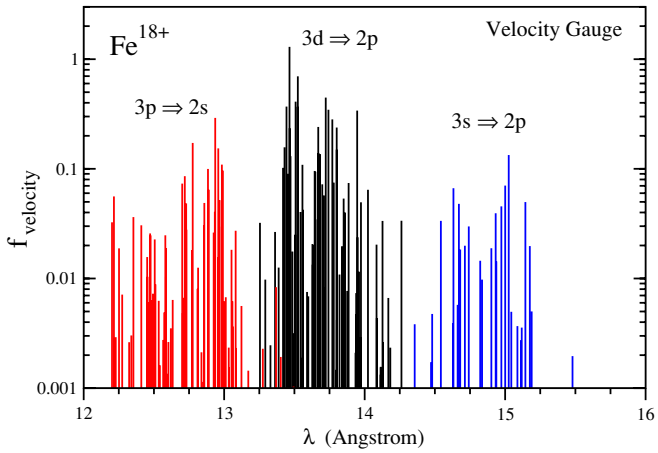

Figure 4. Oscillator strengths of Fe^{18+} for $3p \rightarrow 2s$ (red lines), $3d \rightarrow 2p$ (black lines), and $3s \rightarrow 2p$ (blue lines) transitions as a function of transition wavelength. The oscillator strengths are given in velocity gauge.

(A color version of this figure is available in the online journal.)

well as the three orbital angular momenta of the $n = 3$ shell. The $1s^2 2s^2 2p^4$ ground state configuration of Fe XIX consists of five levels with 2, 1, and 2 levels of total angular momentum $J' = 0$, 1, and 2, respectively. The total number of levels for the excited state configurations is much larger. For example, the $1s^2 2s^2 2p^3 3s$, $1s^2 2s^1 2p^4 3p$, and $1s^2 2s^2 2p^3 3d$ configurations have 10, 42, and 35 levels, respectively.

Table 1 lists our MDFS wavelengths and oscillator strengths for the transition from the $1s^2 2s^1 2p^4 3p$ to the $1s^2 2s^2 2p^4$ configuration. The numerical data for $1s^2 2s^2 2p^3 3s$ and $3d$ levels to the same ground states can be found in Kotochigova et al. (2007). The first three columns of the table give the total angular momentum of the initial and final levels and transition wavelength followed by the oscillator strength in both the velocity and length gauge. Comparison of the two oscillator strengths shows that the uncertainty is generally 2%–3% for most of the transitions from $1s^2 2s^1 2p^4 3p$ to $1s^2 2s^2 2p^4$.

Figure 3 shows a comparison of our MDFS transition wavelengths for Fe XIX with experimental observations (Brown et al. 2002; Shirai et al. 2000) as well as with HULLAC

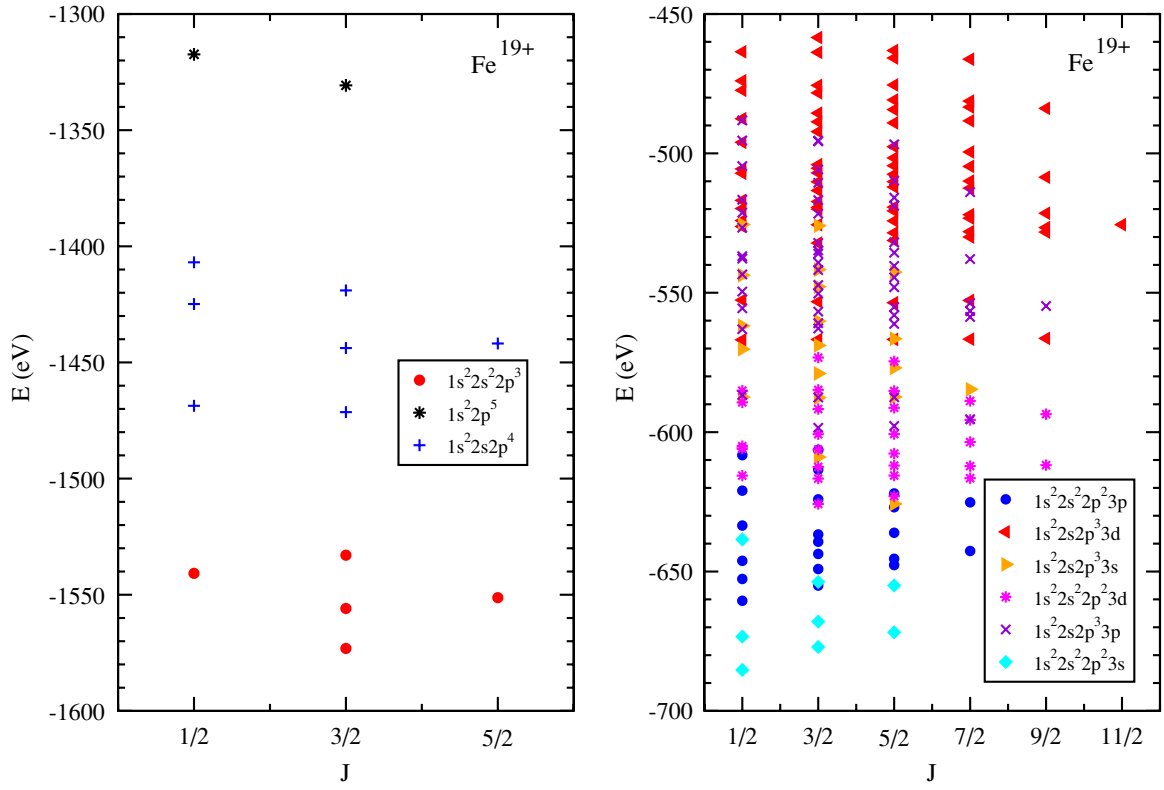

Figure 5. Binding energies for Fe^{19+} levels with respect to the ionization limit, corresponding to an Fe^{20+} ion at a total energy $E_{tot} = -25{,}590.818$ eV plus a free electron at rest. Ground and low-lying states are shown in the left panel and higher-lying states in the right panel.

(A color version of this figure is available in the online journal.)

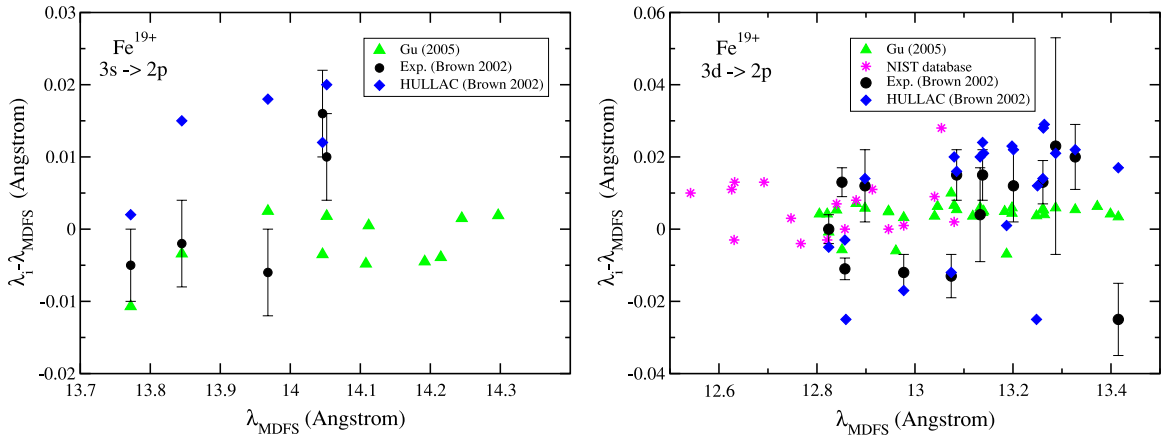

Figure 6. Differences in wavelengths of the $1s^2 2s^2 2p^2 3s \rightarrow 1s^2 2s^2 2p^3$ and $1s^2 2s^2 2p^2 3d \rightarrow 1s^2 2s^2 2p^3$ transitions in Fe^{19+} between our theoretical predictions and experimental and other theoretical results. The keys are explained in the caption of Figure 3.

(A color version of this figure is available in the online journal.)

calculations presented in Brown et al. (2002), the heuristic analyses of Bhatia et al. (1989), and ab initio results of Gu (2005). The transitions from the $1s^2 2s^2 2p^3 3s$ and $3d$ excited levels to the ground $1s^2 2s^2 2p^4$ states are shown. For the $1s^2 2s^1 2p^4 3p$ to $1s^2 2s^2 2p^4$ transition, no such comparison could be made because other data are not available. The overall agreement of our data with the theoretical results of Bhatia et al. (1989) and Gu (2005) is on the order of a few mÅ. The wavelengths predicted by HULLAC are longer by at least 20 mÅ. With the exception of two transitions, the experimental data agree with our theoretical values within the experimental error bars.

Oscillator strengths in the velocity gauge for the $3s \rightarrow 2p$, $3p \rightarrow 2s$, and $3d \rightarrow 2p$ transitions as a function of transition wavelength are given in Figure 4. Three groups of transitions are indicated, showing the overall distribution of oscillator strengths in the X-ray spectra of Fe XIX. The oscillator strengths vary over 3 orders of magnitude.

2.2. *Analysis of the Fe XX Data*

Figure 5 shows our energy levels of the ground and excited states of Fe XX. The ground $1s^2 2s^2 2p^3$ state of Fe XX consists of five levels. The total energy and the value of the Breit and quantum electrodynamic contributions for these levels of the ground configuration are shown in Table 2.

Many more levels are associated with the excited state configurations. For example, for the $1s^2 2s^2 2p^2 3s$, $1s^2 2s^1 2p^3 3p$, and $1s^2 2s^2 2p^2 3d$ configurations there are eight, 52, and

Table 3
X-ray Wavelengths and Oscillator Strengths of Fe XX

J	J'	λ (Å)	$f_{\rm velocity}$	$f_{\rm length}$	λ (Å)	λ (Å)	λ (Å)	λ (Å)
		Current MDFS Data			Exp[a]	HULLAC[a]	NIST[b]	Gu[c]
				$1s^2\ 2s^2\ 2p^2\ 3s \rightarrow 1s^2\ 2s^2\ 2p^3$				
0.5	1.5	13.267	0.000003	0.000003				
1.5	1.5	13.488	0.000239	0.000238				
2.5	1.5	13.506	0.001784	0.001782				
0.5	1.5	13.516	0.000640	0.000642				
1.5	1.5	13.700	0.000474	0.000474				
0.5	0.5	13.743	0.028430	0.028470				
1.5	1.5	13.745	0.011960	0.011940				
2.5	1.5	13.759	0.046100	0.046130				
2.5	1.5	13.772	0.020890	0.020910	13.767(5)	13.774		13.7613
0.5	1.5	13.781	0.000015	0.000015				
1.5	2.5	13.816	0.003251	0.003241				
2.5	2.5	13.837	0.034980	0.034990				
1.5	1.5	13.845	0.030640	0.030660	13.843(6)	13.860		13.8416
0.5	1.5	13.863	0.014490	0.014510				
1.5	1.5	13.965	0.010780	0.010800				
0.5	1.5	13.968	0.018930	0.018950	13.962(6)	13.986		13.9705
1.5	0.5	13.981	0.005233	0.005252				
2.5	1.5	14.029	0.000004	0.000004				
1.5	2.5	14.046	0.036360	0.036350	14.062(6)	14.062		14.0425
0.5	1.5	14.052	0.037180	0.037190	14.062(6)	14.072		14.0538
2.5	2.5	14.108	0.008667	0.008678				14.1032
1.5	1.5	14.112	0.056550	0.056690				14.1125
1.5	1.5	14.112	0.003240	0.003244				
2.5	1.5	14.126	0.013040	0.013090				
1.5	2.5	14.192	0.001849	0.001849				14.1875
1.5	0.5	14.215	0.039020	0.039160				14.2111
0.5	1.5	14.245	0.003147	0.003150				14.2465
0.5	0.5	14.297	0.022890	0.022970				14.2989
1.5	1.5	14.338	0.008903	0.008937				
1.5	0.5	14.358	0.000307	0.000308				
2.5	1.5	14.402	0.000019	0.000020				
0.5	1.5	14.426	0.000088	0.000090				
1.5	1.5	14.489	0.000427	0.000429				
0.5	0.5	14.496	0.000561	0.000563				
0.5	1.5	14.630	0.000037	0.000038				
				$1s^2\ 2s^1\ 2p^3\ 3p \rightarrow 1s^2\ 2s^2\ 2p^3$				
0.5	1.5	11.7289	0.00769	0.00787	11.732(7)	11.730		
2.5	1.5	11.7545	0.07503	0.07636	11.762(5)	11.754	11.760	11.7628
1.5	1.5	11.7976	0.00304	0.00311	11.796(10)	11.786		11.7941
0.5	1.5	12.5194	0.00378	0.00379	12.526(6)	12.591		
0.5	1.5	12.5603	0.05755	0.05778				12.5687
2.5	1.5	12.5714	0.17040	0.17120	12.576(5)			12.5802
1.5	1.5	12.5727	0.11340	0.11400	12.576(5)			12.5813
1.5	1.5	12.6063	0.00072	0.00071		12.602		
2.5	1.5	12.7951	0.00367	0.00366				12.8036
2.5	1.5	12.9315	0.00035	0.00035				12.9394
3.5	2.5	12.9637	0.00001	0.00001				12.9704
1.5	0.5	13.1500	0.00000	0.00000				13.1688
				$1s^2\ 2s^2\ 2p^2\ 3d \rightarrow 1s^2\ 2s^2\ 2p^3$				
1.5	1.5	12.400	0.000003	0.000003				
2.5	1.5	12.415	0.000189	0.000187				
1.5	1.5	12.540	0.000090	0.000092			12.552	
0.5	1.5	12.547	0.001565	0.001570				
2.5	1.5	12.548	0.013970	0.013970				
0.5	1.5	12.601	0.000579	0.000580				
1.5	1.5	12.615	0.003256	0.003260				
2.5	1.5	12.626	0.005422	0.005428			12.637	
1.5	1.5	12.631	0.004601	0.004601			12.628	
2.5	1.5	12.632	0.001762	0.001758			12.645	
1.5	2.5	12.675	0.001383	0.001381				
2.5	2.5	12.692	0.019880	0.019860			12.705	
2.5	1.5	12.747	0.044860	0.044790			12.75	
1.5	1.5	12.749	0.005484	0.005478				

Table 3
(Continued)

J	J'	λ (Å)	f_{velocity}	f_{length}	λ (Å)	λ (Å)	λ (Å)	λ (Å)
		Current MDFS Data			Exp[a]	HULLAC[a]	NIST[b]	Gu[c]
1.5	1.5	12.766	0.005495	0.005473				
0.5	1.5	12.769	0.046970	0.046930				
2.5	1.5	12.767	0.120000	0.120000			12.763	
0.5	1.5	12.805	0.198100	0.197900				12.8092
1.5	0.5	12.813	0.648300	0.647700				
0.5	1.5	12.816	0.078000	0.077960				
1.5	1.5	12.821	0.483700	0.483500			12.818	12.8252
0.5	1.5	12.824	0.082650	0.082630	12.824(4)	12.819		12.8232
1.5	2.5	12.827	0.024900	0.024890				
2.5	2.5	12.832	0.006368	0.006362				
2.5	1.5	12.851	0.463500	0.463400			12.847	12.8453
2.5	1.5	12.857	0.331300	0.331100	12.864(4)	12.854		
1.5	1.5	12.859	0.278000	0.277900	12.846(3)	12.834	12.857	
3.5	2.5	12.880	0.824600	0.824300		12.894	12.888	12.8871
2.5	1.5	12.898	0.193300	0.193300	12.90–12.93	12.912		12.9038
1.5	1.5	12.904	0.017470	0.017480				
2.5	2.5	12.913	0.263200	0.263100			12.924	
1.5	1.5	12.917	0.096280	0.096160				
1.5	2.5	12.919	0.046420	0.046390				
0.5	1.5	12.946	0.008523	0.008512				12.9508
2.5	1.5	12.946	0.115200	0.115200			12.946	12.9510
1.5	1.5	12.961	0.051900	0.051830				
1.5	0.5	12.968	0.070390	0.070380				
0.5	0.5	12.972	0.023420	0.023400				
3.5	2.5	12.972	0.087900	0.087890				
2.5	1.5	12.977	0.640300	0.639700	12.965(5)	12.960	12.978	12.9802
1.5	1.5	12.978	0.000027	0.000027		12.978		
0.5	0.5	13.029	0.165000	0.164700				
0.5	1.5	13.036	0.000443	0.000443				
2.5	2.5	13.040	0.119600	0.119600			13.049	13.0436
1.5	2.5	13.041	0.017090	0.017100				
2.5	1.5	13.046	0.107400	0.107400	12.992(6)	12.988		13.0523
0.5	1.5	13.049	0.000160	0.000161				
1.5	1.5	13.054	0.000206	0.000207			13.082	
1.5	0.5	13.062	0.131000	0.131000				
2.5	1.5	13.074	0.001261	0.001252	13.061(6)	13.062		
1.5	1.5	13.073	0.364000	0.363800				
0.5	1.5	13.077	0.107400	0.107300				
2.5	1.5	13.074	0.519800	0.519400				13.0840
3.5	2.5	13.080	0.259600	0.259500		13.100	13.082	13.0866
1.5	1.5	13.085	0.019930	0.019900	13.100(7)	13.101		13.0904
1.5	2.5	13.118	0.015390	0.015370		13.142		13.1216
2.5	1.5	13.133	0.109900	0.109900	13.137(13)	13.153		13.1389
0.5	1.5	13.137	0.000068	0.000071				
2.5	2.5	13.138	0.056930	0.056910	13.153(7)	13.162		13.1426
1.5	1.5	13.140	0.106200	0.106100		13.161		13.1450
2.5	1.5	13.164	0.036340	0.036400				
1.5	1.5	13.170	0.010690	0.010700				
2.5	1.5	13.183	0.008460	0.008439				13.1879
0.5	1.5	13.184	0.003390	0.003382				
1.5	0.5	13.187	0.512200	0.511500		13.188		13.1801
1.5	1.5	13.198	0.013260	0.013270		13.221		13.2024
2.5	2.5	13.198	0.015290	0.015290				13.2039
3.5	2.5	13.201	0.000011	0.000013	13.213(10)	13.223		
1.5	2.5	13.205	0.002574	0.002577				
0.5	0.5	13.250	0.071240	0.071150		13.262		13.2517
2.5	2.5	13.248	0.000983	0.000976		13.223		
0.5	0.5	13.261	0.133400	0.133400	13.274(6)	13.275		13.2666
3.5	2.5	13.262	0.011510	0.011510		13.290		13.2673
1.5	2.5	13.264	0.012550	0.012540		13.293		13.2680
1.5	0.5	13.265	0.000983	0.000979				
2.5	1.5	13.287	0.024370	0.024380	13.28–13.34	13.308		13.2929
2.5	1.5	13.297	0.009430	0.009348				
1.5	1.5	13.298	0.031680	0.031660				
1.5	1.5	13.327	0.019030	0.019000	13.347(9)	13.349		13.3324

Table 3
(Continued)

J	J'	λ (Å)	$f_{\rm velocity}$	$f_{\rm length}$	λ (Å)	λ (Å)	λ (Å)	λ (Å)
		Current MDFS Data			Exp[a]	HULLAC[a]	NIST[b]	Gu[c]
1.5	0.5	13.354	0.027750	0.027730				
2.5	2.5	13.354	0.002801	0.002799				
0.5	1.5	13.358	0.005315	0.005312				
0.5	1.5	13.372	0.018680	0.018700				13.3783
1.5	1.5	13.377	0.000247	0.000250				
1.5	2.5	13.395	0.000322	0.000322				
2.5	1.5	13.398	0.001330	0.001321				
0.5	0.5	13.399	0.014140	0.014110				13.4032
1.5	0.5	13.415	0.026110	0.026050	13.40–13.38	13.432		13.4184
2.5	1.5	13.460	0.004795	0.004787				
1.5	1.5	13.467	0.006936	0.006940				
0.5	1.5	13.513	0.003065	0.003062				
2.5	1.5	13.513	0.000556	0.000556				
1.5	1.5	13.528	0.013630	0.013620				13.5327
1.5	0.5	13.548	0.001936	0.001926				
2.5	1.5	13.623	0.000005	0.000005				
1.5	1.5	13.665	0.000745	0.000745				

Notes. Transition wavelengths and oscillator strengths from fine structure levels of the excited $1s^2\ 2s^2\ 2p^2 3s$, $3p$, and $3d$ configurations to those of the ground $1s^2 2s^2 2p^3$ or low-excited $1s^2 2s^1 2p^4$ states of Fe xx. Columns labeled J and J' describe the total electron angular momentum of the excited and ground states, respectively. The columns labeled λ, $f_{\rm velocity}$, and $f_{\rm length}$ are the transition wavelengths (in Angstrom) and oscillator strengths in the velocity and length gauge, respectively.

[a] Brown et al. (2002).

[b] Shirai et al. (2000).

[c] Gu (2005).

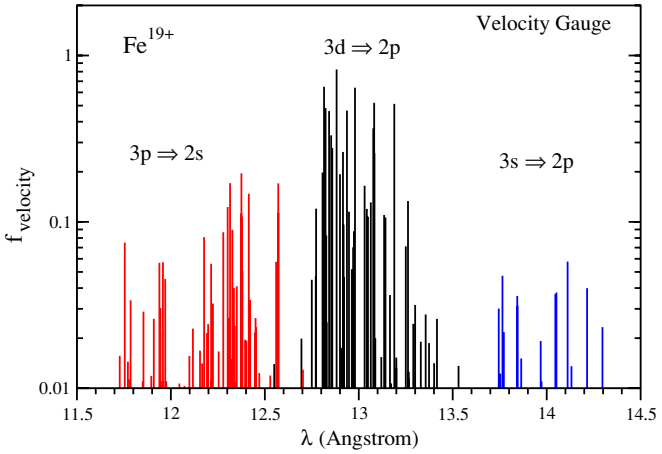

Figure 7. Oscillator strengths of Fe^{19+} for $3p \rightarrow 2s$ (red lines), $3d \rightarrow 2p$ (black lines), and $3s \rightarrow 2p$ (blue lines) transitions as a function of wavelength. The oscillator strengths are given in velocity gauge.

(A color version of this figure is available in the online journal.)

28 levels, respectively. Table 3 shows a comparison of our results with transition wavelengths and oscillator strengths. In addition to the labels of the levels, Table 3 includes experimental and theoretical wavelengths from previous work, when available.

A comparison of the oscillator strengths in the length and velocity gauge allows us to conclude that the uncertainty in our calculated oscillator strengths is less than 1%. In the sixth and seventh columns, we list EBIT measurements and HULLAC calculations from Brown et al. (2002). The results from NIST compilations of Fe xx (Shirai et al. 2000) and the theoretical calculations of Gu (2005) are shown in the last two columns of Table 3.

Figure 6 (left panel) shows a comparison of our $3s \rightarrow 2p$ transition wavelengths with other theoretical and experimental results. Only lines for which a comparison is possible are shown. The two lines with λ = 14.062 Å, which are marked as weak lines in Brown et al. (2002), have the largest discrepancy (0.01–0.02 Å). The wavelengths of the other stronger lines observed by Brown et al. (2002) agree to better than a few times 0.001 Å. The transition wavelengths from HULLAC, which have been used for the identification of the EBIT data, are consistently larger than our MDFS data by about 0.02 Å. Gu (2005) published a larger data set than available from either EBIT or HULLAC. It is, however not a complete listing of allowed $3s$ to $2p$ transitions. A comparison of our data and Gu's shows that our data have smaller transition wavelengths with the exception of the line at 13.763 Å, where we agree to 0.002 Å. On average, the difference in wavelength is 0.006 Å.

For the $3p \rightarrow 2s$ transitions there are only five experimentally observed and assigned lines. Table 3 shows our data for these transitions and a comparison with experimental observations of (Brown et al. 2002), the database of Shirai et al. (2000), and with other theoretical results. The list of the $3p \rightarrow 2s$ transitions in Table 3 is far from complete. The table shows the twelve lines for which in our MDFS calculation the oscillator strengths in the two gauge forms agree well. For the remaining 42 lines, we could not obtain a consistent value for the oscillator strengths in the two gauges. The agreement in the wavelengths of our data with the two measurements (Brown et al. 2002; Shirai et al. 2000) and with the calculations of Brown et al. (2002) and Gu (2005) varies from 0.001 Å to 0.01 Å.

The strongest L-shell lines of Fe xx are identified as $3d \rightarrow 2p$ transitions near 12.85 Å (Brown et al. 2002). Table 3 presents a complete list of these transitions calculated in the current study as well a comparison with the previously mentioned publications. Figure 6 (right panel) gives a graphical representation of the wavelength comparison. Again the discrepancies with other theory (Gu 2005) do not exceed 0.01 Å and with the

experimental data from Brown et al. (2002) and Shirai et al. (2000) are within 0.001 Å to 0.05 Å.

Figure 7 shows the oscillator strengths for Fe XX in velocity gauge. Three groups of transitions are indicated. The strongest are those from $3d \rightarrow 2p$, while the weakest transitions will not be visible on a linear scale. These graphs give a good overview of our predictions.

3. CONCLUSION

X-ray spectra and images of astrophysics objects that have been provided by the *Chandra* satellite have unprecedented clarity and resolution. In order to understand the physical characteristics of these astrophysical observations, very accurate and detailed calculations of the ionic spectra are needed. Here we present results of such calculations for two iron ions, Fe XIX and Fe XX, to be used in future analyses. A good example of our successful modeling of the observed spectra is presented in Figure 1 (lower panel), where our wavelengths were used to calculate an Fe XIX emission spectrum of Capella.

S.K. and M.L. acknowledge partial support from the Smithsonian Institution Atherton Seidell Fund through the Smithsonian Astrophysical Observatory. N.S.B. acknowledges support from NASA contract NAS8-03060 to the Chandra X-ray Center.

REFERENCES

Bhatia, A. K., Fawcett, B. C., Lemen, J. R., Mason, H. E., & Phillips, K. J. H. 1989, MNRAS, 240, 421
Brickhouse, N. S. 2007, in AIP Conf. Proc. 926, Atomic Processes in Plasmas, ed. J. D. Gillaspy, J. J. Curry, & W. L. Wiese (Melville, NY: AIP), 102
Brillouin, L. 1932, J. Phys., 7, 373
Brinkman, A. C., et al. 2001, A&A, 365, L324
Brown, G. V., Beiersdorfer, P., Liedahl, D. A., Widmann, K., Kahn, S. M., & Clothiaux, E. J. 2002, ApJS, 140, 589
Canizares, C. R., et al. 2000, ApJ, 539, L41
Chen, G. X. 2008, MNRAS, 386, L62
Desai, P., et al. 2005, ApJ, 625, L59
Gu, M. F. 2005, ApJS, 156, 105
Hubac, I., & Wilson, S. 2000, J. Phys. B, 33, 365
Kotochigova, S., Kirby, K. P., & Tupitsyn, I. I. 2007, Phys. Rev. A, 76, 052513
Krongold, Y., Nicastro, F., Brickhouse, N. S., Elvis, M., Liedahl, D. A., & Mathur, S. 2003, ApJ, 597, 832
Lennard-Jones, J. E. 1930, Proc. R. Soc. A, 129, 598
Miller, J. M., Wojdowski, P., Schulz, N. S., Marshall, H. L., Fabian, A. C., Remillard, R. A., Wijnands, R., & Lewin, W. H. G. 2005, ApJ, 620, 398
Ness, J.-U., Brickhouse, N. S., Drake, J. J., & Huenemoerder, D. P. 2003, ApJ, 598, 1277
Pollock, A. M., Corcoran, M. F., Stevens, I. R., & Williams, P. M. 2005, ApJ, 629, 482
Shirai, T., Sugar, J., Musgrove, A., & Wiese, W. L. 2000, J. Phys Chem. Ref. Data, Monograph 8; http://physics.nist.gov/PhysRefData/ASD/index.html
Smith, R. K., Brickhouse, N. S., Liedahl, D. A., & Raymond, J. C. 2001, ApJ, 556, L91
Wigner, E. P. 1935, Math. Naturw. Anz. Ungar. Akad. Wiss., 53, 475